Boundary layer transition over a low reynolds number rotor: effects of roughness and freestream turbulence

Thomas Jaroslawski, Maxime Forte, Jean-Marc Moschetta, Erwin Gowree

Association Aéronautique et Astronautique de France

56th 3AF International Conference on Applied Aerodynamics
28 — 30 March 2022, Toulouse – France

FP97-2022-jaroslawski

BOUNDARY LAYER TRANSITION OVER A LOW REYNOLDS NUMBER ROTOR: EFFECTS OF ROUGHNESS AND FREESTREAM TURBULENCE

Thomas Jaroslawski[1*], Maxime Forte[1], Jean-Marc Moschetta[2], Erwin Gowree[2]
*[1]ONERA, DMPE, Universite de Toulouse, 31055, Toulouse, France . thomas.jaroslawski@onera.fr**
[2]ISAE-SUPAERO, Universite de Toulouse, 31055, Toulouse, France

ABSTRACT

Two separate experiments are conducted on a three bladed NACA0012 rotor operating at low Reynolds numbers using phase-locked infrared thermography coupled with simultaneous force and torque measurements. The first, focuses on the effects of freestream turbulence on boundary layer transition over the suction side of the aerofoil of the rotor in an advancing configuration. Freestream turbulence (FST) was generated in an open section wind tunnel using grids and was characterized using Hot-Wire anemometry. In general, when the rotor was subjected to FST, an increase in thrust and efficiency was observed, which could be due to the FST suppressing flow separation or by inducing early transition. The second experiment, consisted of a parametric study on the impact of forcing boundary layer transition using roughness placed on the suction side of the aerofoil, in a hover configuration. The height of the roughness was varied from 52-220μm and was placed at all at at 10% chord, over the entire span of the blade. Force and torque measurements revealed that there could be a optimal roughness height that could lead to a performance increase.

1. INTRODUCTION

Further knowledge of low Reynolds number flows is becoming increasingly important due to the rise in the demand of micro-aerial vehicles (MAV). This encourages us to rethink the way conventional aerodynamic design is conducted, as these vehicles operate within a Reynolds number ($Re = U_{tip}c/\nu$, where c denotes, ν the kinematic viscosity and for a rotor blade: $U_{tip} = R\Omega$, where R is the blade radius and Ω is the rotational speed.) regime of $10^3 < \mathrm{Re} < 10^5$ where one can expect that the flow remains laminar to a greater extent but is still susceptible to transition. With MAV systems projected to operate in highly turbulent environments understanding the impact of boundary layer transition becomes critical for the design of low Reynolds number flyers as it could lead to considerable deterioration in performance or in worst case scenarios, massive stall and control loss as they are more prone to separation in the low Reynolds number regime.

Flow separation is an important factor in low Reynolds number aerofoil design philosophy, while trying to extend the amount of laminar flow and delaying transition to turbulence when skin friction drag reduction is necessary. For example, Singh and Ahmed [19] took a lamianr separation bubble (LSB) into consideration when designing a low Reynolds number wind turbine and noted that LSBs over low Reynolds number rotors cause excessive pressure drag, loss in aerodynamic lift and increase the noise produced by the rotor. A recent study, on a rotor blade similar to that of the NASA Mars helicopter, by Argus et al.[1], used mid-fidelity RANS simulations coupled with a Blade Element Momentum Theory model to find that at Re = 2×10^4 and 8×10^4 increasing the critical N-factor (the amount of perturbation growth required for transition) from 3 to 11 decreased the figure of merit (FM) of the rotor by approximately 40% suggesting that a performance gain is possible. They noted that in their configuration laminar separation without reattachment was the transition mechanism that deteriorated performance.

Contemporary boundary layer transition research on rotors most commonly uses infra-red thermography (IRT), where investigations on laminar to turbulent transition in rotary wing configurations entail more experimental difficulties than in fixed wing configurations. Lang et al.[14] used IRT and PIV to detect the presence of an LSB over a NACA 0015 rotor blade, showing that, the elevated temperature region could be used to deter-

mine the location of the bubble(the local *Re* at which the bubble was measured was 1.4×10^5). Recently, Thiessen and Shülein [20] conducted transition experiments over a low Reynolds number quadcopter rotor using IRT and oil film topography measurements. They found a region of separated flow, which they claimed to be an LSB that forms over the rotor blade. The laminar separation bubble is a zone of almost stationary or low speed reverse flow, where the shear stress is zero or very low. In the separation region the heat transfer will be minimal and will begin to increase rapidly as transition and turbulent reattachment take place. In general, IR measurements conducted on a model which has a higher surface temperature than the free stream allows for identification of turbulent regions (low temperature, low pixel intensity, I_N), separated regions (high temperature, high values of I_N) and laminar regions (medium temperature regions). In our recent investigations by Jaroslawski et al. [10, 9] IRT was used coupled with force and torque measurements to characterize the flow topology and performance of a NACA0012 rotor operating at low Reynolds numbers. Boundary layer transition was fostered using large (with respect to the boundary layer thickness) 2D and 3D roughness elements, resulting in a general decrease in performance, which was attributed to increased excrescence drag caused by the roughness elements. Furthermore, it was demonstrated that IRT measurements could provide qualitative quantification of the flow topology, with a possible region of separated flow being present.

Further investigation needs to be conducted on effects of perturbations on the flow development over rotors operating at low Reynolds number, as previous investigators [10, 13, 19] have shown that the state of the boundary layer can have a significant impact on performance. The lack of parametric experimental investigations on boundary transition is addressed in this paper, with the objectives consisting of studies on the effects of different boundary layer forcing techniques on the flow topology and performance, more specifically:

1) What is the impact of freestream turbulence on the performance of a rotor in climb operating at low Reynolds numbers?

2) What is the effect of varying the roughness height of 3D roughness elements on the performance and flow development/topology of the rotor ?

2. EXPERIMENT AND METHODS

The experiments were conducted at the Institut Supérieur de l'Aéronautique et de l'Espace (ISAE-SUPAERO) with the collaboration of ONERA in Toulouse, France. The rotor had three blades with a NACA0012 profile, an angle of incidence of 10 $^\circ$ and no twist. The radius (R) of the rotor was 0.125 m and the chord length (c) was 0.025 m, resulting the in rotor having an aspect ratio ($AR = R/c$) of 5. The rotor blades were 3D printed using a reinforced resin, great care was taken to ensure that the blade was smooth. The rotor was placed in a recirculating open test section wind tunnel with an estimated level of freestream turbulence intensity (Tu) of 0.42%. The experimental setup is presented in Fig.1. Two separate experiments were conducted, the first consisted of the rotor in the climb condition subjected to a freestream flow velocity of $U_o = 4\ m/s$ and varying levels of freestream turbulence generated by regular square grids (cf. Fig.2a). Free stream turbulence measurements were conduced using a 5 μm Dantec 55P11 probe, where a 6 mm diameter Dantec 55H24 probe support was used to support the X-wire probes. All test data were acquired using a National Instruments CompactDAQ-9178 with two NI-9239 (built in resolution of 24 bit) modules for voltage measurements. The hotwire was calibrated *insitu* against a pitot tube connected to a MKS 220DD pressure transducer, using King's law [2].

The second experiment, consisted of a parametric investigation on the rotor in the hover configuration ($U_o = 0m/s$, ie. wind tunnel shut off) subjected to forcing via 3D roughness (circular cylinders). The roughness elements were placed at $x/c = 0.1$ on the suction side of each blade, and had a heights (k) varying from 52-220μm. The performance of the rotor was measured with force and torque measurements and the flow development/topology on the suction side of the aerofoil was captured with IRT. The thrust and torque were measured using the same aerodynamic balance as in Desert et al. [3], which used load cells to measure the thrust and torque. To measure the thrust, one end of the load cell was fixed to the motor driving the rotor and the other to a fixed support. The torque was obtained by fixing one end of the load cell to a circular plate fixed to the back of the motor (aligned with the axis of rotation) and the other to a fixed frame surrounding the motor. The frame allows for free rotation of the motor along its axis through two ball bearings. Therefore when a torque is applied, it pushes onto the load cell. It must be noted, that the experimental setup measured the sum of the aerodynamic torque exerted by the rotor on the motor and the internal mechanical torque of the motor. The sampling frequency of the force and torque measurements was 500 Hz, 5000 samples were acquired, with a 10 second stabilization period between each speed interval. The force and torque were measured for long enough so that their means and standard deviations converged. The uncertainty of the thrust and torque measurements was calculated using a 95% confidence interval, the total uncertainty for the thrust and torque was approximately 1% and 0.045 % of full scale, respectively. Using a similar experimental setup as in Jaroslawski et al. [9, 10], phase locked IRT was used to capture the temperature distribution of the rotor blade's surface. A Brüel Kjær CCLD laser tacho probe was used

to synchronize the blade with the IR Camera. A thin reflective film was placed on an opposing blade, so that for each rotation a voltage pulse was sent out by the laser to trigger the camera. In order to increase the temperature difference between the ambient air and the blades surface, a 500W halogen lamp was used to increase the surface temperature of the blade of interest. Before starting the measurement, the blade of interest was systematically heated by the lamp at a distance of 0.15 m for 10 seconds. The room temperature was at 20 °C and the blade was heated to approximately 35-40 °C in each case, however the absolute temperature is not of great importance as the transition detection techniques are based on temperature differences. Energy injected into the flow due to heating of the blade can affect the critical Reynolds number at which boundary layer transition occurs [18], however this is mainly relevant for modal transition which is bypassed when transition occurs immediately downstream of a 3D roughness. Furthermore, the heating is too low to affect the transition process, especially at the low Reynolds numbers studied, where the boundary layer is much more stable. In previous work, the overheat temperature employed was between 10-20 °C, where [17, 15, 22] suggested that these levels of overheat do not significantly affect transition position.

Furthermore, The Richardson number can be used to address the extent of the relevance of natural convection to forced convection. The Richardson number is defined in Eq. 1, where θ, represents the volumetric thermal expansion coefficient ($105\times10^{-6}/C^{\circ}$), the rotational acceleration is defined as $a = U_{tip}^2/r$ and used instead of the acceleration due to gravity as rotational accelerations would dominate. The surface temperature of the model and the ambient air temperature are denoted by T_w and T_∞, respectively.

$$Ri = c\theta(T_w - T_\infty)/r \tag{1}$$

Natural convection can be considered to be negligible if $Ri < 0.1$, in the present work $Ri \sim 0.0032$ at r/R = 0.1 and decreases as r/R is increased, therefore natural convection effects on the flow can be neglected. During the IR camera measurement the heating lamp was turned off, the motivation of this technique is that in a turbulent flow region there will be more heat transfer between the wall and outer flow than in a laminar flow region. Therefore the temperature (pixel intensity) will vary in a turbulent, laminar or separated region as a function of time. Since a variety of configurations were tested, a pixel intensity normalization technique needed to be implemented for coherent analysis. Each IR image was normalized by the maximum pixel intensity present in the image so that the different test configurations would be compared reliably. The high speed and high resolution IR camera (Infratec) was used to characterize the flow topology over the rotor, where the pixel intensity is used to approximate the state of the boundary layer. The camera has a 320 × 256 pixel MCT sensor having a nominal Noise Equivalent Temperature Difference (NETD) $< 20mK$ and was positioned 0.4m away from the rotor blade and at a horizontal angle of 25° (cf. Fig.1. The size of the field of view was 1c x 0.8R and the exposure time of the camera was 68μs, allowing for a good compromise between camera noise and motion blur. Since the camera was synchronized with the rotor, effectively, the sampling rate was that of the rotors turning rate (RPM) for the given run. Motion blur is one of the greatest challenges when conducting IR measurements, even with state-of-the-art cameras. The Motion blur can be calculated by multiplying the exposure time of the camera by the local radial velocity. Increasing the rotational speed and radial position results in more blur. For example at the highest speed, 5000 RPM and at the blade tip, the motion blur can be up to 0.18c, however this value is less than 0.1c for a large portion of the blade as the radial velocity decreases moving inboard. When raw images were analyzed the blur was not significant enough to affect the test result potentially due to the reliable synchronisation. Furthermore, at lower rotational speeds, the blur is between 0.01c and 0.1c, depending on speed and radial position.

2.1 Freestream turbulence configurations

The free stream turbulence is characterised by its intensity (Tu) and streamwise integral length scale (Λ_u). The integral length scale is the most energetic scale, corresponding to the average size of the average energy containing eddy. Freestream turbulence was generated using a variety of static turbulence generating grids. Different grid soldities (σ), mesh sizes (M), bar thickness (t) and relative distances between the grid and the leading edge can be used to vary the FST characteristics. In the present work σ was held constant and M was varied to change the levels of turbulence intensity. Turbulence grids which have a small M, reach equilbrium after a shorter stream wise distance, hence, have low streamwise variation of Tu. All grids were placed at least $15M$ away of from the rotor, ensuring the FST is relatively isotropic and homogeneous. The Tu is defined in Eq. 2.

$$Tu = \frac{u_{rms}}{U_0} \tag{2}$$

The Λ_u are calculated by integrating the auto correlation of their fluctuating velocity signals and applying Taylor's hypothesis of frozen turbulence, which converts time scales to spatial scales where $f(\tau)$ is the auto correlation of the fluctuating velocity signal and τ is the time delay, and is presented in Eq. 3:

$$\Lambda_u = U_0 \int_0^\infty f(\tau) d\tau \tag{3}$$

where $f(\tau)$ denotes auto correlation function of the signal and τ the time delay. The the grid parameters

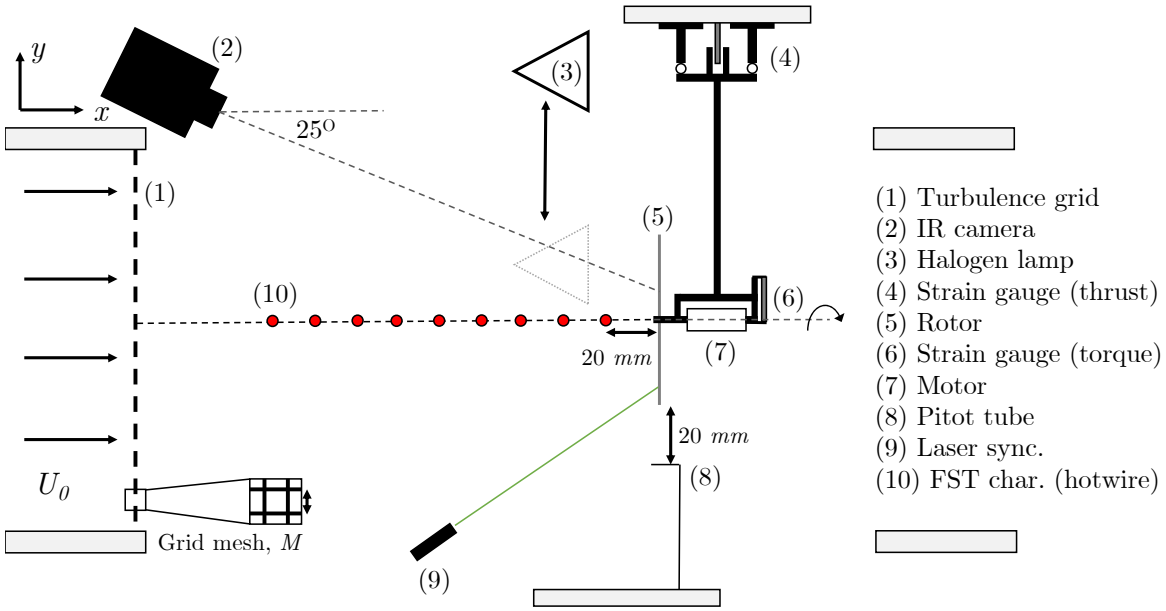

Figure 1: Experimental Setup

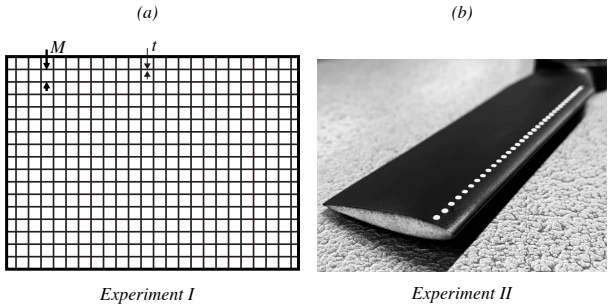

Figure 2: Forcing methods used in the study. (a) 3D printed regular turbulence generating

along with their corresponding values of Tu and Λ_u are presented in Table 1. The spanwise homogeneity of the mean flow and turbulence was verified with hotwire measurements, however for the sake of brevity are not presented here.

Cfg.	$M(mm)$	$t(mm)$	x/M	$Tu(\%)$	$\Lambda_u(mm)$
G1	12	1	20	4.91	4.24
G2	18	2	16	6.38	8.01

Table 1: Grid and turbulence characteristics at the leading edge of the rotor. Both grids had values of $\sigma = 0.34$.

2.2 Roughness configurations

Due to the experimental difficulty in measuring the boundary layer thickness (δ) over a small-scale rotating surface, the δ is estimated numerically. The purpose of estimating the boundary layer thickness was to compare it to the height of the roughness, and to estimate U_k the undisturbed velocity at the roughness height, to calculate the roughness Reynolds number, Re_k. The pressure over the surface of the rotor was calculated using XFOIL [4] for the local Reynolds number based on local radial speed and the effective aerodynamic angle of attack (α_{eff}) for the corresponding radial position and rotation speed was calculated using a Non Linear Vortex Lattice Method (NLVLM) which should take into account some of the 3D effects present, the method is explained in detail in Jo et al. [11]. Using the pressure obtained XFOIL (calculated with an N-Factor of 7), the δ was calculated using ONERA's in house boundary layer code 3C3D, which solves Prandtl's boundary layer equations for three-dimensional boundary layers using a method of characteristics along local streamlines. To set up the boundary layer equations a body fitted coordinate system is used and the momentum equations are discretized along the local streamlines [8, 16].

A frequently used criterion for determining the critical roughness size of three-dimensional roughness was given by Von Doenhoff and Braslow [21] based on a limited body of experimental observations. In Von Doenhoff and Braslow [21], the roughness Reynolds number is introduced as, $Re_k = U_k k/\nu$, where k is the roughness height and U_k. By its nature, such a criterion, does not address the problem of shape and distribution of the roughness elements, however should suffice for the objectives of this current work. From Von Doenhoff and Braslow [21] the critical roughness Reynolds number for turbulent wedge

formation (Cf. [10, 21, 6] for more details) is defined as:

$$Re_{k,crit} \approx 600(d/k)^{-2/5} \tag{4}$$

where d denotes the diameter of the roughness element. Using the boundary layer computations (3C3D), the approximated range of δ/k along span of the rotor blade and $Re_{k,crit}$ for the roughness configurations is pretested in Tab. 2. In addition to the criteria proposed by Von Doenhoff and Braslow [21], Gregory and Walker [7] conducted experiments using isolated roughness elements at various heights, both smaller and larger than δ. They found that at $\sqrt{Re_k} \approx 25$ a turbulent wedge would form immediately downstream the roughness element. Furthermore, they also studied roughness elements which were over 2δ and found that the turbulent wedge would increase in spanwise size near the roughness element. The values of $Re_{k,crit}$ and the boundary layer thickness with respect to the roughness are presented in Table 2

k	$\sqrt{Re_{k,crit}}$	$k/\delta_{3000RPM}$	$k/\delta_{5000RPM}$
52μm	12.92	0.01-0.21	0.11-0.27
78μm	14.02	0.14-0.32	0.17-0.40
140μm	15.75	0.26-0.57	0.31-0.72
220μm	17.25	0.41-0.89	0.48-1.13

Table 2: Summary of roughness configurations tested. Where the range in δ/k corresponds to $r/R = 0.2-0.95$. All roughness elements are located at $x/c = 0.1$.

3. RESULTS AND DISCUSSION

3.1 Freestream Turbulence

The characterisation of the freestream turbulence is presented in Fig 3, where the streamwise evolution of the Tu (cf. Fig. 3a) with the exponential decay being present before the leading edge of the rotor and the integral length scales increasing in size further away from the grid (not presented here). The Power Spectral Density (PSD) in Fig .3b, of the streamwise fluctuating velocity, exhibits a broader inertial sub-range for the configuration with a higher level of Tu, which is coherent with the values of Λ_u.

The coefficient of thrust (C_T) and efficiency (η), Power Loading (PL) and efficiency are defined in Eqs. 5, 6, and 7, respectively. Where T is the thrust, Q is the torque, ρ is the density of the ambient air, Ω is the rotational frequency, R is the rotor blade radius and U_0 is the incoming velocity.

$$C_T = \frac{T}{\rho(\Omega R)^2 \pi R^2} \tag{5}$$

$$PL = \frac{T}{\Omega Q} \tag{6}$$

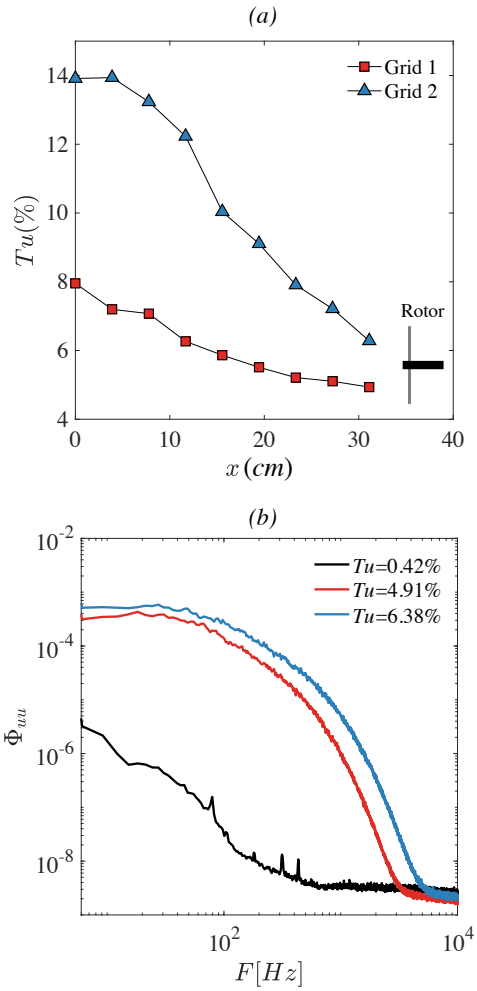

Figure 3: (a) Streamwise evolution of the turbulence intensity Tu and (b) Power Spectral Density 20 mm before the rotor

$$\eta = \frac{TU_0}{2\pi\Omega Q} \tag{7}$$

Referring to the C_T, η and PL presented in Fig. 4, increasing the level of freestream turbulence in general improves the performance. The effects of FST on the C_T are less pronounced at lower rotational speeds where at speeds of $2600-3200RPM$ there is a slight decrease in the evolution of C_T with no effects of FST on the performance being present. This could be due to the the local angle of incidence not being positive along the entire span of the rotor in this range of Ω, causing " locally negative thrust", which contributes to a slight decrease in the total drag. Once $\Omega > 3200RPM$, the angle of attack is positive along the entire span of the rotor and the effects of FST become more pronounced. The mechanism behind the performance increase cannot be fully explained based on the current measurements. However, based on the low Reynolds number and previous investigations [19, 1]

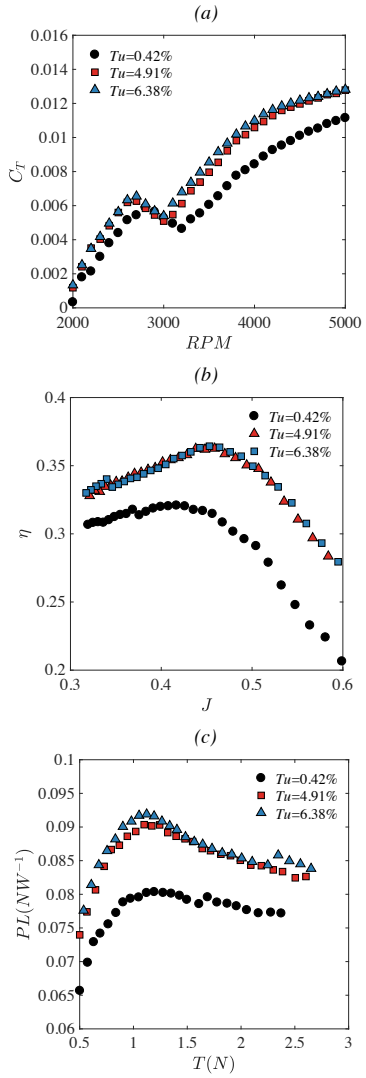

Figure 4: (a) The coefficient of thrust (C_T), (b) Efficiency (η) and (c) Power Loading (PL) for the rotor in the climb configuration. The advance parameter is defined as $J = nU_o/2R$

boundary separation is possible in the current configuration, leading to a hypothesis consisting of the FST interacting with the boundary layer developing over the rotor. The increased energy in the boundary layer could excite the flow, which would, in turn, delay or suppress flow separation. The effects of the turbulence on the drag of the rotor and support were also investigated, and it was found that the drag execrated by the freestream flow on both was relatively constant over all turbulence configurations, indicating the FST could be indeed interacting with the boundary layer developing over the surface of the aerofoil. Further IRT measurements should be conducted to investigate the flow topology over the rotor in the presence of FST, however it is unsure whether turbulent streaks (commonly present in high levels of FST [5]) could be measured as the Reynolds number is low, hence the temperature gradient between the low and high momentum zones was too small to measure.

3.2 Roughness configurations

The C_T, Figure of Merit (FM) and PL are presented in Fig. 5, where the FM is defined, *viz*,

$$FM = \frac{T^{3/2}}{\Omega Q \sqrt{2\rho\pi R^2}} \tag{8}$$

Upon inspection of the C_T, FM and PL, it can be observed that the addition of roughness can have a twofold effect on the performance. Roughness elements with smaller wall-normal distance (52 and 78 μm) show an increase in performance and whereas those with higher wall normal distances (140 and 220 μm) deteriorate the performance. A deterioration in the performance a low Reynolds number rotor with roughness elements was observed by Jaroslawski et al. [10] where it was postulated, that very large roughness elements could cause increased levels of excrescence drag. On the other hand, increased levels of rotor performance was observed by Jung and Baeder [12], who conducted numerical simulations on a wind turbine rotor and found that forcing transition with optimal distributed surface roughness affects the performance differently depending on the state of the boundary layer. They found that in the presence of separated flows the addition of upstream roughness could increase the performance up to 23.3% whereas it would result in a decrease of 8.3% for an attached flow. Recent numerical simulations on a rotor similar to the NASA Mars helicopter by Argus et al. [1] at Re $\leq 1 \times 10^5$, representative of the current experiment, showed that early transition caused by a decreased critical amplification factor resulted in a thrust increase through the elimination of laminar separation. At higher *Re* the benefit of early transition diminished and became detrimental for the thrust produced by the rotor. They showed that the FM could be increased by 40% when the N-factor which is a measure of the growth rate of the perturbation in boundary layers.

IR snapshots of the flow topology over the rotor for each roughness configuration, along with radial evolution of the Roughness Reynolds number (Re_k) at $x/c = 0.1$, which was calculated using the boundary layer profiles calculated with 3C3D are presented in Fig. 6. IR snapshots show the formation of undeveloped turbulent turbulent streaks and at a critical value ofRe_k, breakdown into turbulent wedges. Referring to Fig. 6, the Von Doenhoff and Braslow [21] criterion can provide an approximation for when roughness elements will cause the flow to transition. For example, at 3000 *RPM* (cf. Fig. 6a) Re_k does not reach a critical value for roughness heights of 52 and 78μm resulting in no clear wedge formation

behind the roughness elements. Furthermore, increasing Ω to 5000 RPM increases the Re_k to critical value for the 78 configuration, resulting in wedge formation at approximately the critical value proposed by Von Doenhoff and Braslow [21]. Additionally, the performance increase is only present when $Re_k < Re_{k,crit}$, suggesting $Re_{k,crit}$ could be used as a threshold for "overtripping", in terms of performance.

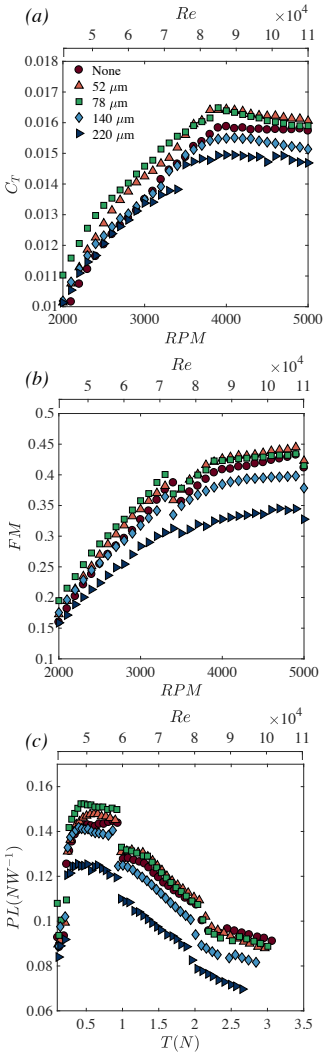

Figure 5: (a) The coefficient of thrust (C_T), (b) Figure of Merit (FM) and (c) Power Loading (PL) for the rotor in the hover configuration.

4. CONCLUSION

Infrared thermography coupled with force and torque measurements on a rotor operating at low Reynolds numbers were conducted. The effects of freestream turbulence and roughness revealed that:

1) Freestream turbulence can increase the performance (C_T, η and PL) of a rotor operating at low Reynolds numbers ($40000 < Re < 110000$). The possible mechanisms behind the performance increase could be a delay/suppression of boundary layer separation via freestream turbulence, due to the energy in the freestream exiting the boundary layer. Further investigation should be conducted in characterising the transition mechanisms of the boundary layer developing over the rotor when subjected to freestream turbulence.

2) 3D roughness placed at the $x/c = 0.10c$ can have a twofold effect on the performance, with the roughness Reynolds number (Re_k) being a critical parameter. Criteria proposed by [21] work reasonably well in determining when turbulent wakes caused by the 3D roughness elements breakdown into turbulence. Configurations which values of Re_k were found to increase performance, suggesting that when $Re_k \approx Re_{k,crit}$ the excrescence drag caused by the roughness can be detrimental. The mechanisms of performance increase could be due to delay/suppression of boundary layer separation as suggested by [1, 12].

The present results could indicate that exciting the boundary developing over the suction side of a NACA0012 rotor operating at low Reynolds numbers can increase the performance. In particular, the FST being efficient in boundary layer forcing as the boundary layer is energized without the addition of excrescence drag as with the use of roughness elements, where a incorrectly designed element can decrease the performance. However, the current results also suggest that it is possible to design an optimal roughness trip which can lead to a performance increase.

REFERENCES

[1] Finbar J Argus, Geoffrey A Ament, and Witold JF Koning. The influence of laminar-turbulent transition on rotor performance at low reynolds numbers. *VFS Technical Meeting on Aeromechanics for Advanced Vertical Flight,San Jose, CA, January 21–23, 2020*, 2020.

[2] Hans H Bruun. Hot-wire anemometry: principles and signal analysis, 1996.

[3] T Desert, JM Moschetta, and H Bezard. Aerodynamic design of a martian micro air vehicle. In *Proceedings of the 7th European Conference for Aeronautics and Aerospace Sciences*, 2017.

[4] Mark Drela. Xfoil: An analysis and design system for low reynolds number airfoils. In *Low Reynolds number aerodynamics*, pages 1–12. Springer, 1989.

[5] Jens HM Fransson, Masaharu Matsubara, and P Henrik Alfredsson. Transition induced by freestream turbulence. *Journal of Fluid Mechanics*, 527:1–25, 2005.

[6] David Goldstein, Jeff Chu, and Garry Brown. Lateral spreading mechanism of a turbulent spot and a turbulent wedge. *Flow, Turbulence and Combustion*, 98(1):21–35, 2017.

[7] NT Gregory and WS Walker. *The effect on transition of isolated surface excrescences in the boundary layer*. HM Stationery Office, 1956.

[8] R Houdeville. Three-dimensional boundary layer calculation by a characteristic method. In *Fifth Symposium on Numerical and Physical Aspects of Aerodynamic Flows, Long Beach, January 1992*, 1992.

[9] Thomas Jaroslawski, Maxime Forte, Gregory Delattre, Erwin Ricky Gowree, and Jean-Marc Moschetta. Laminar to turbulent transition over a rotor at low reynolds numbers. In *Aero 2020+ 1-55th 3AF International Conference on Applied Aerodynamics*, pages FP94–2020, 2020.

[10] Thomas Jaroslawski, Maxime Forte, Jean-Marc Moschetta, Gregory Delattre, and Erwin R Gowree. Characterisation of boundary layer transition over a low reynolds number rotor. *Experimental Thermal and Fluid Science*, 130:110485, 2022.

[11] Yeongmin Jo, Thierry Jardin, Romain Gojon, Marc C Jacob, and Jean-Marc Moschetta. Prediction of noise from low reynolds number rotors with different number of blades using a non-linear vortex lattice method. In *25th AIAA/CEAS Aeroacoustics Conference*, page 2615, 2019.

[12] Yong Su Jung and James Baeder. Simulations for effect of surface roughness on wind turbine aerodynamic performance. In *Journal of Physics: Conference Series*, volume 1452, page 012055. IOP Publishing, 2020.

[13] Witold JK Koning, Ethan A Romander, and Wayne Johnson. Low reynolds number airfoil evaluation for the mars helicopter rotor. 2018.

[14] W Lang, AD Gardner, S Mariappan, C Klein, and M Raffel. Boundary-layer transition on a rotor blade measured by temperature-sensitive paint, thermal imaging and image derotation. *Experiments in Fluids*, 56(6):118, 2015.

[15] Massimo Miozzi, Alessandro Capone, Marco Costantini, Lorenzo Fratto, Christian Klein, and Fabio Di Felice. Skin friction and coherent structures within a laminar separation bubble. *Experiments in Fluids*, 60(1):13, 2019.

[16] J Perraud, O Vermeersch, and R Houdeville. Descriptif et mode d'emploi du code 3c3d. *ONERA, RT*, 1:18325, 2011.

[17] Markus Raffel and Christoph B Merz. Differential infrared thermography for unsteady boundary-layer transition measurements. *AIAA journal*, 52(9):2090–2093, 2014.

[18] P Schäfer, J Severin, and H Herwig. The effect of heat transfer on the stability of laminar boundary layers. *International journal of heat and mass transfer*, 38(10):1855–1863, 1995.

[19] Ronit K Singh and M Rafiuddin Ahmed. Blade design and performance testing of a small wind turbine rotor for low wind speed applications. *Renewable Energy*, 50:812–819, 2013.

[20] Raffael Thiessen and Erich Schülein. Infrared thermography and dit of quadcopter rotor blades using laser heating. In *Multidisciplinary Digital Publishing Institute Proceedings*, volume 27, page 31, 2019.

[21] Albert E Von Doenhoff and Albert L Braslow. The effect of distributed surface roughness on laminar flow. In *Boundary layer and flow control*, pages 657–681. Elsevier, 1961.

[22] Dallyn W Wynnychuk and Serhiy Yarusevych. Characterization of laminar separation bubbles using infrared thermography. *AIAA Journal*, 58(7):2831–2843, 2020.

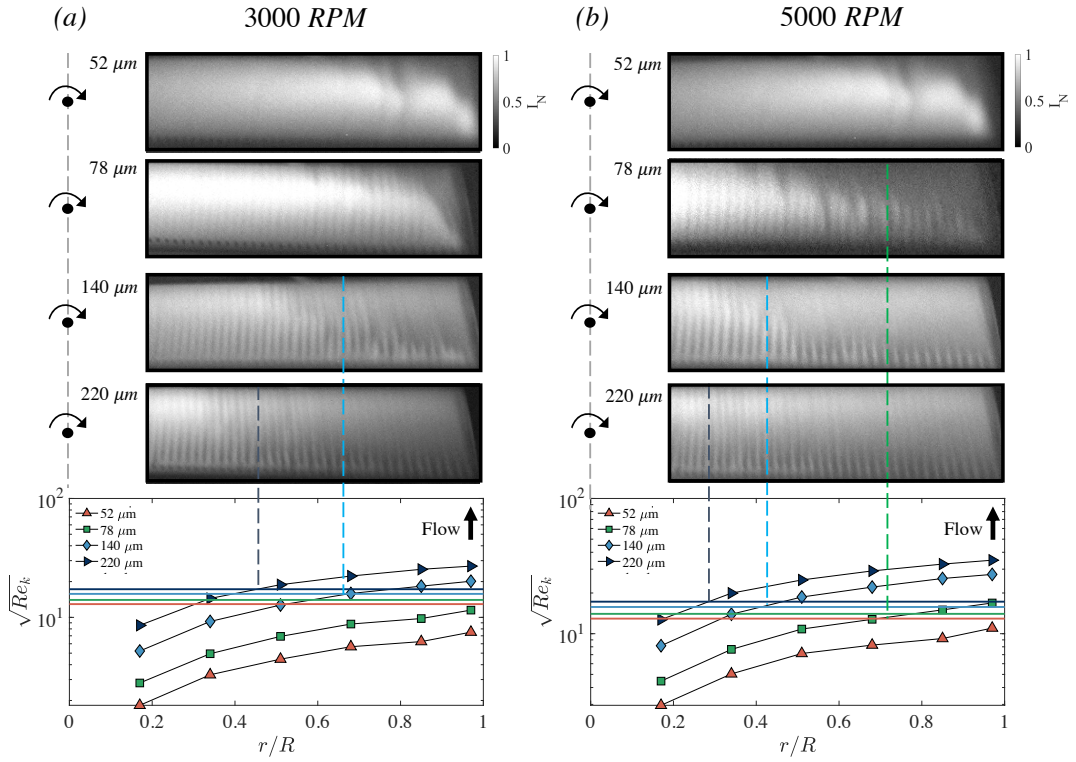

Figure 6: Normalised IR snapshots and the evolution of the radial roughness Reynolds number (Re_k) for (a) 3000 RPM and (b) 5000 RPM. NB the horizontal lines denote the critical roughness Reynolds number for each roughness configuration [21]